The Astronomical Journal, 138:1655–1660, 2009 December doi:10.1088/0004-6256/138/6/1655

XMM-NEWTON OBSERVATIONS OF SDSS J143030.22−001115.1: AN UNUSUALLY FLAT-SPECTRUM ACTIVE GALACTIC NUCLEUS

S. Mathur[1], E. C. Golowacz[1], R. Williams[2], R. Pogge[1], D. Fields[3], and D. Grupe[4]
[1] Department of Astronomy, The Ohio State University, Columbus, OH 43210-1173, USA
[2] Leiden Observatory, Leiden 2300RA, Netherlands
[3] L.A. Pierce College, Woodland Hills, CA 91371, USA
[4] Pennsylvania State University, State College, PA, USA
Received 2009 May 27; accepted 2009 September 30; published 2009 October 29

ABSTRACT

We present *XMM-Newton* observations of the type 1 active galactic nucleus (AGN) SDSS 1430−0011 ($z = 0.1032$). The low signal-to-noise ratio spectrum of this source obtained in a snap shot *Chandra* observation showed an unusually flat continuum. With the follow-up *XMM-Newton* observations, we find that the source spectrum is complex; it either has an ionized absorber or a partially covering absorber. The underlying power law is in the normal range observed for AGNs. The low flux of the source during *Chandra* observations can be understood in terms of variations in the absorber properties. The X-ray and optical properties of this source are such that it cannot be securely classified as either a narrow-line Seyfert 1 or a broad-line Seyfert 1 galaxy, adding to the group of sources in the "in-between" class.

Key words: galaxies: active – galaxies: individual (SDSSJ143030.22−001115.1) – galaxies: nuclei – X-rays: galaxies

1. INTRODUCTION

Narrow-line Seyfert 1 galaxies (NLS1s) were initially classified by Osterbrock & Pogge (1985) as a peculiar subset of active galactic nuclei (AGNs) with strong, narrow Hβ emission (FWHM(Hβ) $\leqslant$ 2000 km s^{-1}), relatively weak [O III], and strong optical Fe II emission. These spectral properties cause NLS1s to stand out at one extreme end of the Boroson & Green (1992) "Eigenvector 1" (EV1). The physical driver behind EV1 is debated, but is usually thought to correlate with the Eddington luminosity ratio, $L_{\rm bol}/L_{\rm Edd}$. NLS1s then lie at the extreme end of EV1 corresponding to high $L_{\rm bol}/L_{\rm Edd}$ (Pounds et al. 1995) and also seem to have lower black hole masses than broad-line AGNs of similar luminosities (Grupe et al. 2004, and references therein).

Subsequent X-ray studies found that many NLS1s have unusual X-ray properties as well (e.g., Puchnarewicz et al. 1992). NLS1s often exhibit rapid, short timescale variability (Boller et al. 1996) which is consistent with their having small mass black holes. Sometimes they also display large amplitude variability (Boller et al. 1996). In a detailed study of variability property of NLS1s, Leighly (1999a) found that at a given X-ray luminosity, NLS1s are significantly more variable than BLS1s. Again, this may be interpreted as NLS1s having smaller BH masses and higher accretion rates relative to Eddington compared to BLS1s. As a class, NLS1s also exhibit ultrasoft ($\Gamma \gtrsim 2.5$) X-ray spectra compared to "normal" Seyfert 1s (Boller et al. 1996), while some also show soft X-ray emission in excess of that expected from a power law (Leighly 1999b). Kuraszkiewicz et al. (2000) noted that this ultrasoft X-ray emission may be a consequence of high accretion rates, and a correlation between $L_{\rm bol}/L_{\rm Edd}$ and Γ is indeed observed in the Grupe (2004) sample. Mathur (2000) proposed that the high accretion rate and low black hole mass indicate that NLS1s are "young" AGN; i.e., the central black holes are in an early stage of their growth. It was later found that NLS1s tend to fall below the $M_{\rm bh}$–σ relation observed for broad-line Seyfert 1s supporting this idea (Mathur et al. 2001) and bringing up the intriguing possibility that AGNs are "born" off of the $M_{\rm bh}$–σ relation and eventually grow onto it through accretion (Grupe & Mathur 2004; Mathur & Grupe 2005a, 2005b; Watson et al. 2007).

Because of these properties, soft X-ray selection has proven to be an efficient technique for finding large numbers of NLS1s (Grupe et al. 2004). However, the aggregate X-ray properties of NLS1s cannot be easily studied with soft X-ray-selected samples because these necessarily exclude any NLS1s with harder X-ray emission, if they exist. These issues were partially resolved by the Sloan Digital Sky Survey (SDSS) with its homogeneous selection criteria, and in particular by the subsample of Williams et al. (2002, hereafter W02) selected from the SDSS solely on the basis of the Osterbrock & Pogge (1985) optical spectral criteria. Indeed, the NLS1s from that sample which also appeared in the *ROSAT* All-Sky Survey (RASS) have on average flatter spectra than soft X-ray-selected samples (W02).

A substantial number of NLS1s in the W02 sample should have been detected in the RASS based on their optical brightness, but were not. Short (2 ks) observations of 17 of these X-ray-faint NLS1s were taken with *Chandra* in a follow-up study (Williams et al. 2004, hereafter W04). Some of these objects exhibit X-ray properties typical of NLS1s, with $\Gamma \sim 2$–3 and X-ray to optical luminosity ratios consistent with the RASS-detected NLS1s in W02. However, four of the NLS1s in the W04 sample are detected as unusually hard and faint sources, with $\Gamma < 2$ inferred from the *Chandra* spectral fit or hardness ratio (HR; see below for details). Additionally, those objects with low Γ tend to be much fainter in X-rays than the average for RASS-detected NLS1s and the high-Γ W04 NLS1s.

From works of W02 and W04, it is quite clear that NLS1s are much more heterogeneous in their accretion properties than previously thought; i.e., even though NLS1s *as a class* have high $L_{\rm bol}/L_{\rm Edd}$, not all NLS1s do (see also Nikolajuk et al. 2009). Some NLS1s have steep X-ray spectra, but some do not. Some NLS1s have strong Fe II emission, but some do not. It does appear that, for the most part, NLS1s with large $L_{\rm bol}/L_{\rm Edd}$ have steep Γ (Grupe 2004) and strong Fe II emission, and those

are the objects whose black holes are still growing (Mathur & Grupe 2005a, 2005b). Of the four flat-spectrum NLS1s in W04, two are very peculiar (SDSS J143030.22−001115 and SDSS J1259+0102) with inferred $\Gamma = 0.92 \pm 0.64$ and $0.25^{+0.80}_{-1.01}$, respectively, much too flat even for normal Seyfert 1 galaxies which have average $\Gamma \approx 2$.

The original classification of SDSS J143030.22−001115.1 (SDSS J1430−0011 here after) as a NLS1 was based on the SDSS spectrum (W02). Bian et al. (2006) analyzed this spectrum again and found that if you remove the narrow components of Hβ, the remaining broad component has FWHM = 2600–2900 km s^{-1} (dependent upon exact modeling). Since the formal definition of NLS1 (Goodrich 1989) has a maximum width of 2000 km s^{-1}, Bian et al. argue that SDSS 1430−0011 is not a NLS1. Even if SDSS J1430−0011 is a BLS1 or a NLS1 (discussed further in Section 5.1), the *Chandra* spectrum with $\Gamma = 0.92$ is still peculiarly flat.

In principle, the apparent low X-ray luminosities and low photon indices seen in either of these AGNs could be caused by high intrinsic column density or variability (though it is unlikely that both would be in such a low state during both the RASS and *Chandra* observations). Unfortunately, the individual *Chandra* spectra of the four hardest NLS1s contained too few counts to constrain both $N_{\rm H}$ and Γ, but a stacked spectrum of all four showed no evidence for strong absorption ($N_{\rm H} < 2 \times 10^{21}$ cm^{-2} at the 2σ confidence level). A high signal-to-noise ratio (S/N) spectrum is clearly required to understand whether the spectrum is truly flat or appears flat due to complexity.

We were awarded 25 ks of *XMM-Newton* time to obtain a high S/N spectrum of SDSS J1430−0011 ($z = 0.1032$). In *Chandra* observations, the source was found to be faint, with count rate, CR = 0.012 counts s^{-1}. W04 characterized its spectrum in terms of the hardness ratio, defined as HR = $\frac{(H-S)}{(H+S)}$, where H and S are the net counts in the hard and soft bands, respectively (the hard band is defined as 2 keV $< E <$ 8 keV and the soft band as 0.4 keV $< E <$ 2 keV). They found HR = −0.25. They also fit a simple power law to *Chandra* data, fixing the absorption column density to the Galactic value, and infer $\Gamma = 0.92 \pm 0.64$. In the following, we present *XMM-Newton* observations of this source.

2. OBSERVATIONS AND DATA REDUCTION

The NLS1 SDSS J1430−0011 was observed with the *XMM-Newton* European Photon Imaging Camera (EPIC) pn and MOS detectors on 2008 January 6 for a total of 25 ks. All instruments were observed in extended full frame mode with thin filters.

2.1. Data Preparation

The *XMM-Newton* data were reduced using Science Analysis System (SAS) 7.1.0. Light curves were initially produced for both EPIC pn and MOS images in order to check for flaring high background. Periods of high background are typically produced by protons in the Earth's atmosphere with energies $\lesssim$100 keV which are funneled toward the detectors by the X-ray mirrors.[5]

Low background intervals were then produced by excluding data taken when the full-field CRs exceeded 20 s^{-1} in the pn and 2.5 s^{-1} in the MOS. Photon pile-up was also checked for, and was determined not to be a problem. Images were produced and binned into square pixels of 4″. Source and background data were then extracted.

[5] *XMM-Newton* Users' Handbook: http://xmm.esa.int/external/xmm_user_support/documentation/uhb/XMM_UHB.html

Table 1
SDSS J1430−0011, Obs ID 05015402 Details

Instrument	Exposure Time (ks)[a]	Count Rate($\times 10^{-2}$ counts s^{-1})
pn	12.9	6.6 ± 0.2
MOS 1	15.6	1.4 ± 0.1
MOS 2	15.5	1.6 ± 0.1

Note. [a] Effective exposure times after data reduction.

For the EPIC pn data, the source counts were extracted with a circular region of 20″ centered on the object. Since the source was close to a chip gap, background data were extracted from a source free circular region of 20″ on the same CCD at about the same distance from the readout node. Furthermore, the source and background data were filtered to include only single and double events (PATTERN 0-4).

For the MOS data, the source was extracted in a circular region of 20″ centered on the object. The background was extracted in a surrounding annulus of outer and inner radii 50″ and 25″, respectively. Additionally, the source and background data were filtered to include singles, doubles, triples, and quadruples (PATTERN 0-12).

The SAS task *backscale* was then run on both data sets to take into account bad pixels and CCD boundaries. A Redistribution Matrix File and Ancillary Response File were then produced with the tasks *rmfgen* and *arfgen*, respectively. The final effective exposure times and CRs for pn, MOS1 and MOS2 cameras are given in Table 1.

3. DATA ANALYSIS AND MODEL FITTING

The pn and MOS spectra were binned to have a minimum of 30 and 15 counts per bin, respectively, using the FTOOLS program *grppha* and then analyzed using the XSPEC 12.3.1 software package. Joint fits were made to the pn and MOS spectra. We use solar abundances from Lodders (2003) and photoelectric absorption cross sections from Morrison & McCammon (1983). Throughout the data analysis, we use $H_0 = 70$ km s^{-1} Mpc^{-1}, $\Omega_\Lambda = 0.7$, and $\Omega_m = (1 - \Omega_\Lambda) = 0.3$.

We fit a variety of models, all of which are described in detail in the subsections below. In every model, we included absorption by the interstellar medium (ISM) of the Milky Way which was held fixed when fitting the spectrum. The Galactic column density toward SDSS J1430−0011 is $N_{\rm H}^{\rm Gal} = 3.15 \times 10^{20}$ atoms cm^{-2} (Dickey & Lockman 1990). The goodness of fit was determined through χ^2 statistic. The errors quoted are for 90% confidence for one interesting parameter ($\Delta\chi^2 = 2.706$), unless noted otherwise. In Table 2, we list only the acceptable models with their fit parameters.

3.1. Modeling the Data

Before any modeling was done to the *XMM-Newton* data, we applied the results from the *Chandra* observation. We fit our *XMM-Newton* data with a simple power law, and fixed the photon index $\Gamma = 0.92$ (derived in W04). We looked to see how the model behaved, and then made some assumptions about the structure of the continuum and chose additional models accordingly. The flat continuum derived from the *Chandra* data did not match the data at all and indicated that the true spectrum is more complex than a simple power law.

Outlined below are the models we used. Joint fits were made to EPIC pn and MOS spectra for 0.3 keV $\leqslant E \leqslant$ 10 keV. For simplicity, we have included their XSPEC syntax.

Table 2
Model Parameters[a]

Model Name[b]	$N_{\rm H}$ (10^{22} cm^{-2})	Γ	Other Parameter[c]	χ^2_ν/ν	$P_\chi(\chi^2;\nu)$	L_{2-10} ($\times10^{42}$ erg s^{-1})	F_{2-10} ($\times10^{-14}$ erg s^{-1} cm^{-2})
Model 3: ionized absorber	$4.3^{+9.8}_{-2.5}$	2.18 ± 0.14	323^{+976}_{-212}	0.954/58	0.575	2.43	9.08
Model 4: partial covering	$4.47^{+4.78}_{-1.72}$	$2.74^{+0.21}_{-0.20}$	$0.72^{+0.08}_{-0.13}$	1.128/58	0.235	2.12	7.66
Model 5: disk blackbody	...	1.73 ± 0.16	0.118 ± 0.02	0.9236/58	0.640	2.65	10.1

Notes.
[a] This table only lists models that were considered as representative.
[b] Galactic absorption was included in all models and was held fixed.
[c] Ionization parameter ξ in erg cm s^{-1} for Model 3, covering fraction C_f for Model 4, disk temperature in keV for Model 5.

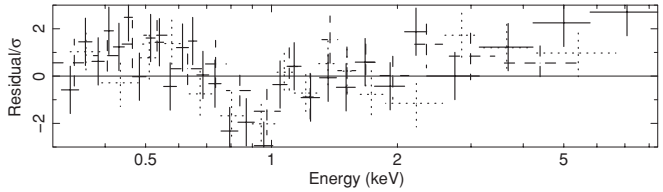

Figure 1. Residuals (σ) to a fit with a simple power-law model (Model 1). Notice the residuals at around 1 keV, suggestive of an ionized absorber.

Model 1: simple power law. This simple photon power-law model (at the redshift of the source) was fitted with the XSPEC command *wabs(zpow)*. The free parameters of the model were the photon index Γ, and the normalization. This was not a good fit, with $\chi^2 = 95.1$ for 60 degrees of freedom. Moreover, the best-fit $\Gamma = 2.3\pm0.1$ is very different from the $\Gamma = 0.92$ derived from the *Chandra* data. The true spectrum of the source, therefore, must be more complex than a simple power law. As shown in Figure 1, the fit left significant negative residuals at around 1 keV. This is suggestive of an ionized absorber along the line of sight; such a model is discussed below.

Model 2: intrinsic absorber. Apparent flatness of a continuum can be caused by incorrect modeling of absorption. To investigate whether this is the case, we next fitted the data with a model with intrinsic absorption and a simple power-law continuum at the redshift of the source (XSPEC model *wabs*zwabs(zpow)*). The free parameters in this model were $N_{\rm H}$, Γ, and the normalization. This model did not result in a good fit either ($\chi^2 = 205$ for 59 degrees of freedom). The residuals to the fit showed excess counts below about 1 keV. This implies that simple absorption by neutral matter at the source is not the cause of the apparent flatness of the *Chandra* spectrum.

Model 3: ionized absorber. This model consists of an ionized absorber with a simple power-law continuum at the redshift of the source (XSPEC model *wabs*absori(zpow)*). The free parameters of this model are $N_{\rm H}$, Γ, the normalization, and absorber ionization state ξ.[6] This resulted in an acceptable fit (Table 2). The best-fit values of the parameters are $\Gamma = 2.18^{+0.13}_{-0.14}$ and the effective column density of the ionized absorber $N_{\rm H} = 4.3^{+9.8}_{-2.5}\times10^{22}$ cm^{-2}. The ionization parameter is $\xi = 323^{+976}_{-212}$ erg cm s^{-1}. The intrinsic power-law slope is in the normal range observed for AGNs. Figure 2 shows the spectral fit of this model.

Model 4: partially covering absorber. The apparently flat spectrum, the excess of counts at low energy in Model 2, and the dip in the residuals to the Model 1 fit, are suggestive of a partially covering absorber, so we try this model next (XSPEC model *wabs*zpcfabs(zpow)*). The free parameters of this model are Γ, the normalization, $N_{\rm H}$, and the covering fraction. The quality of this fit was similarly acceptable to that of Model 3 (Table 2). The best-fit vales of the parameters are $\Gamma = 2.74\pm0.20$ and $N_{\rm H} = 4.47^{+4.78}_{-1.72}\times10^{22}$ cm^{-2}. The covering fraction is $C_f = 0.72^{+0.08}_{-0.13}$. The power-law slope is in the range observed for NLS1s. Figure 3 shows the spectral fit and the confidence contours are shown in Figure 4.

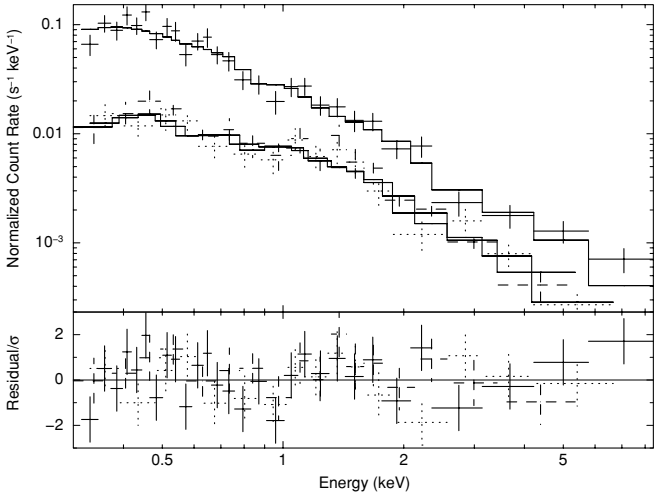

Figure 2. Model of ionized absorber fits the *XMM-Newton* data well (top panel). The solid "+" symbols mark the pn data (upper curve) while the dotted and dashed symbols are for the MOS 1 and 2 data (lower curve). The solid lines running through the data sets correspond to the best-fit model. Residuals to the fit (σ) are plotted in the bottom panel.

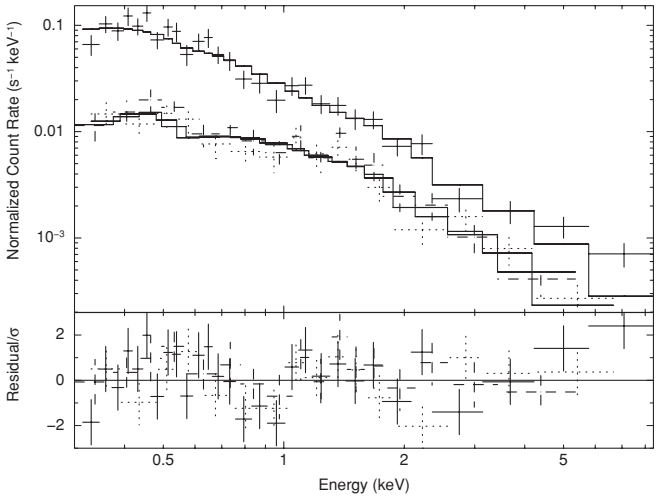

Figure 3. Same as Figure 2, but for a model with a partially covering absorber.

[6] $\xi \equiv \frac{L}{N_e R^2}$, where L is the integrated luminosity from 5 eV to 300 keV, R is the radial distance from the source to the ionized material, and N_e is the number density of electrons (Done et al. 1992). The temperature was held fixed at 3×10^4 K, and the iron abundance was held fixed at the solar value.

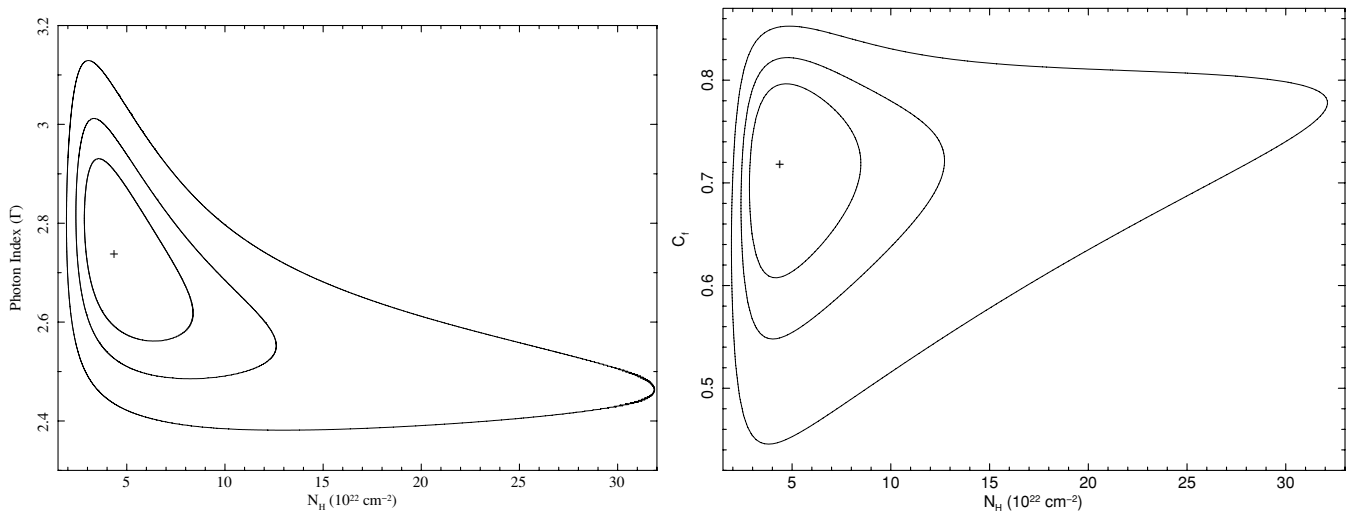

Figure 4. Confidence contours of parameters in Model 4 (partial covering). The best-fit parameters and the one, two and three σ intervals are shown. Left: column density vs. power-law slope Γ. Right: column density vs. covering fraction.

Model 5: disk blackbody. In an attempt to rule out other possible scenarios, we looked at additional models that may also have been representative of our source.

As discussed above, residuals to Model 2 show excess at low energies. Similarly, if we fit the spectrum with a simple power law for $E \geqslant 2$ keV and extrapolate it down to lower energies, we again see an excess in data. This upturn may indicate soft excess which is a characteristic of NLS1s. The cause of the soft excess in NLS1s is a matter of debate (see, e.g., Atlee & Mathur 2009, and references therein). For the purpose of this paper, however, we are only interested in parameterizing the excess, so we looked at blackbody, Comptonization, and thermal plasma models described by Page et al. (2004). Only the disk blackbody model was deemed acceptable based on fit statistics, which is discussed here.

A disk blackbody model describes the emission from an accretion disk as a series of blackbodies at different temperatures, which are emitting from different radii (see Mitsuda et al. 1984; Makishima et al. 1986.), XSPEC model *wabs(zpow+diskbb)*. The free parameters in this model were Γ, the normalizations,[7] and the temperature at the inner disk radius. This model also fit the data well (Table 2). The resulting $\Gamma = 1.73 \pm 0.16$ and the disk temperature is 0.118 ± 0.02 keV.

A flat X-ray spectrum may also imply that the primary continuum is suppressed and the spectrum has a reflection component. However, as shown in Figure 1, the characteristic strong Fe–Kα line and the continuum "hump" of the reflection model in the hard X-rays is not seen. SDSS 1430−0011 is also a type 1 AGN, so unlikely to be completely dominated by a reflection component. Therefore, we do not discuss this model in details. As discussed below, it is clear that the intrinsic spectrum of the source is not flat as inferred from the *Chandra* data. The *XMM-Newton* data, however, cannot distinguish among different complex models; fitting models that are not physically motivated is, therefore, avoided. Moreover, the utility of reflection models to infer underlying physical parameters is limited by the unknown geometry of the reflector (Murphy & Yaqoob 2009).

4. CONSISTENCY WITH *CHANDRA* DATA

As discussed above, the three models listed in Table 2 fit the *XMM-Newton* data well. The correct model of the spectrum of SDSS J1430−0011 should also be consistent with the *Chandra* data. In the disk blackbody model, even the high-energy power -law is as steep $\Gamma = 1.73$, much steeper than the $\Gamma = 0.92$ derived from the *Chandra* data and there is the blackbody excess at low energies. Thus, this model cannot lead to an apparently flat spectrum during *Chandra* observation. Indeed, the best-fit HR of this model is $\mathrm{HR} = -0.61 \pm 0.01$, much softer than observed. For this reason, we do not discuss this model further.

To check the consistency with *Chandra* data for the other two acceptable models (Models 3 and 4), we calculate the predicted *Chandra* ACIS-S CR over the 0.4–8.0 keV range and the corresponding HR; we then compare these parameters with observations. The models were produced in XSPEC and then exported to the Portable, Interactive Multi-Mission Simulator (PIMMS) software version 3.9[8] for predicting CRs and HR. For the best-fit parameters, the predicted *Chandra* CRs are $\mathrm{CR} = 0.022$ counts s^{-1} for Model 3 and $\mathrm{CR} = 0.0228$ counts s^{-1} for Model 4. These are higher than the observed CR of 0.012 counts s^{-1}. A change in column density between the *Chandra* and *XMM-Newton* observations can lead to such a change in the CR. Alternatively, the ionization parameter (Model 3) or the covering fraction (Model 4) could have been different. To investigate whether this is the case, we varied N_{H}, C_f, and ξ in the subsequent analysis, while holding all other parameters of the models fixed.

In Figure 5, we have plotted predicted *Chandra* HR as a function of N_{H} for the partial covering model. The dashed horizontal lines define the 1σ confidence interval of the observed *Chandra* HR. The dashed vertical lines correspond to 90% confidence intervals for N_{H} in the partial covering model. The dotted curves are for a range of C_f as indicated; for each C_f the *Chandra* HR is predicted for a range of N_{H}. As can be clearly seen from the figure, the best-fit values of N_{H} and $C_f (= 0.72)$ are inconsistent with the *Chandra* HR. The best-fit value of

[7] There are two normalizations. One is the normalization of the power law, which is the photon flux per unit energy at 1 keV. The other normalization is associated with the disk blackbody, which is defined to be $\left(\frac{R_{\mathrm{in}}/\mathrm{km}}{D/10\,\mathrm{kpc}}\right)^2 \cos\theta$ where R is an "apparent" inner disk radius, D is the distance to the source, and θ is the angle of the disk ($\theta = 0$ implies face on).

[8] Available at http://heasarc.gsfc.nasa.gov/docs/software/tools/pimms.html.

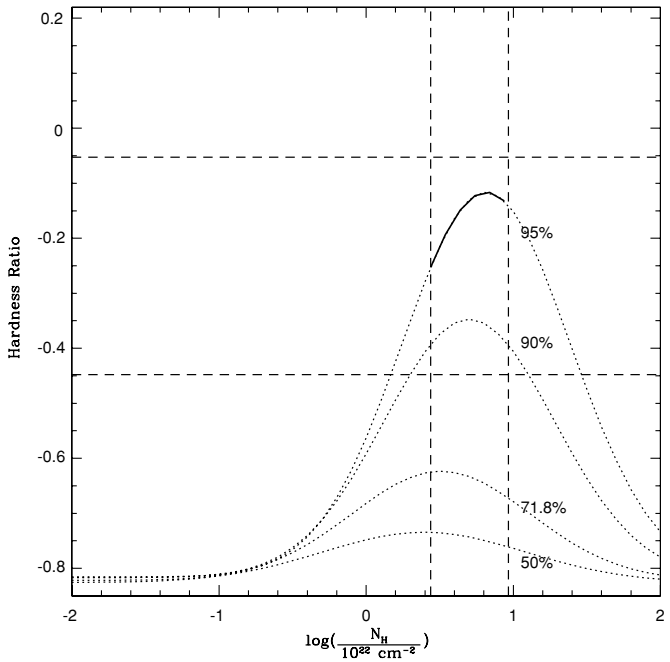

Figure 5. Plot of predicted *Chandra* hardness ratio vs. column density $N_{\rm H}$ for the partial covering model. The dotted curves are for a range of covering fractions as marked: 95%, 90%, 72% (best-fit model), and 50%. The dashed horizontal lines mark the 1σ interval of observed *Chandra* HR. The dashed vertical lines are for the 1σ range of best-fit column density in the partial covering model. The solid line is for the range of parameters consistent with the 2σ–3σ confidence interval of observed *Chandra* count rate.

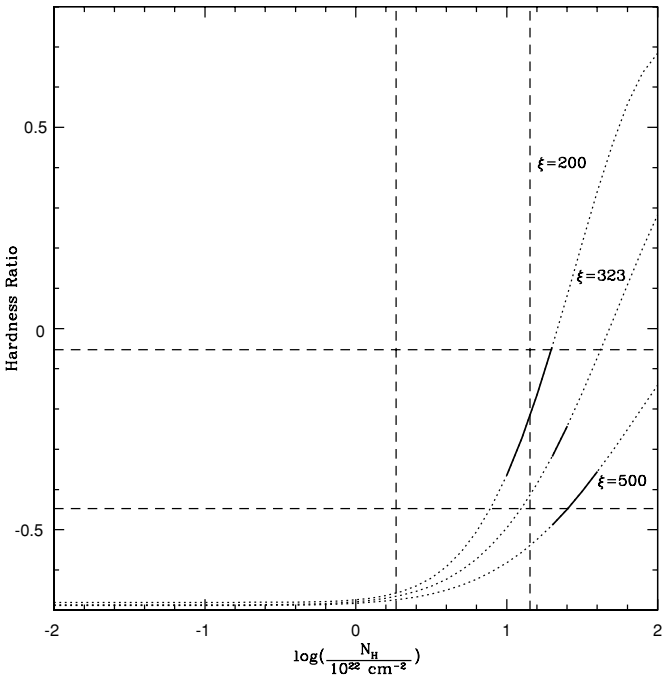

Figure 6. Same as Figure 5, but for the ionized absorber model. The dotted curves are for a range of ξ as labeled: 200, 323 (best fit), and 500. Again, the solid lines represent model parameters consistent with the observed *Chandra* count rate within 1σ confidence.

covering fraction is inconsistent with *Chandra* HR for any $N_{\rm H}$. Thus, the change in CRs between *Chandra* and *XMM-Newton* observations cannot be explained by a simple change in column density. Covering fraction between about 90%–95%, together with the best-fit column density are consistent with the *Chandra* HR. However, the predicted CR for the $C_f = 0.9$ model is CR = 0.019, still above the observed value. On the other hand, if $C_f = 0.95$, then the predicted CR = 0.012, as observed. Thus, if a power law with a partially covering absorber is the correct description of the source spectrum, then the covering fraction must have changed from about 0.95 to 0.72 between *Chandra* and *XMM-Newton* observations.

In Figure 6, we present a similar plot for the ionized absorber model. The dotted curves are for a range of ξ values, as labeled. The solid lines correspond to the parameter space consistent with observed *Chandra* CR. Again, the best-fit values of $\xi(= 323)$ and $N_{\rm H}$ do not match the *Chandra* HR. For the best-fit ξ, higher values of $N_{\rm H}$, between $23.3 < \log N_{\rm H} < 23.4$ match the *Chandra* HR as well as CR. For the observed $N_{\rm H}$, the ionization parameter will have to be as low as $\xi \approx 200$ to match the *Chandra* data. Thus, if an ionized absorber model is the correct description of the target spectrum, the column density had to be higher, or the ionization parameter had to be lower, during the *Chandra* observation.

5. DISCUSSION

The target of our *XMM-Newton* observations, SDSS J141430−0011, showed an unusually flat spectrum and low luminosity during *Chandra* observations. The *XMM-Newton* observations showed that the spectrum is complex; it can be well described by an ionized absorber model or with a partially covering absorber model. The best-fit power-law slopes in both cases were steeper ($\Gamma = 2.18$ and 2.74) respectively. Thus, the intrinsic power-law slope of the source is not flat. The apparent faintness and spectral flatness during the *Chandra* observation can be explained if the covering fraction during the *Chandra* observation was higher than that found during the *XMM-Newton* observation if the partial covering model is correct. Alternatively, if the ionized absorber model is correct, then either the absorber column density was higher or the ionization parameter was lower during *Chandra* observations.

The X-ray luminosity of the source, however, is still low even after proper modeling of the *XMM-Newton* spectrum. With L(2–20 keV) $\approx 2.75 \times 10^{42}$ erg s^{-1}, SDSS J1430−0011 falls below the Grupe (2004) relation between X-ray power-law slope and luminosity. Its Eddington luminosity ratio is also low $L/L_{\rm Edd} \approx 0.1$ for a black hole mass of $\log M_{\rm BH}/M_{\odot} = 6.6$ calculated using Hβ line width, luminosity and the scaling relations (from W04) and assuming that the bolometric luminosity is about $9 \times L$(2–10 keV) (Grupe 2004). It still falls below the W04 relation between optical and X-ray luminosity of RASS-detected sample (the optical luminosity being $\log \lambda L_{\lambda}(5100)$ erg s^{-1} = 43.19). SDSS J1430−0011 thus remains X-ray weak not only compared to normal NLS1s, but also BLS1s, as per the $\log L_X$–$\log \lambda L_{\lambda}(5100)$ correlation in Grupe (2004, his Figure 9).

5.1. Classification of SDSS 1430−0011

Given all its properties, it is worth asking if SDSS 1430−0011 is a bona fide NLS1 galaxy. As discussed in Section 1, Bian et al. (2006) argue that it is not a NLS1. These authors arrived at this conclusion by separating the narrow components of the Hβ line from the broad component and found that the width of the broad component is about 2800 km s^{-1}. They modeled the narrow component based on the [O III] lines. It was also found that the [O III] lines show blue asymmetry, a quality more often found in NLS1s than in BLS1s (Mathur 2000; Komossa & Xu 2007). It is useful, therefore, to examine other properties of this galaxy and compare them with the distributions found

for NLS1s and BLS1s. The S/N in the SDSS spectrum is low, but the high-ionization "coronal" lines of Fe VII λ6087 and Fe X λ6375 are possibly detected in the optical spectrum. NLS1s, with their steep X-ray spectra often show strong coronal lines (e.g., Pfeiffer et al. 2000). The observed X-ray power-law slope is $\Gamma = 2$–2.3 (90% confidence range) for Model 3 and 2.5–2.9 for Model 4. This is consistent with the range found for optically selected NLS1s of W04. It is also consistent with the range of X-ray-selected BLS1s in Grupe et al. (2004). The Fe II/Hβ ratio of the source is 0.59 ± 0.17. This lies in the overlapping region between the peaks of NLS1s and BLS1s in the distribution found by Grupe et al. (2004). At high X-ray luminosities, NLS1s typically show steeper spectra than BLS1s. But at low luminosities, as observed for our source, both NLS1s and BLS1s have $\Gamma \approx 2.5$ (Grupe 2004, their Figure 7). Thus, it appears that SDSS 1430−0011 is at the border line between NLS1s and BLS1s.

SDSS 1430−0011, however, is not alone in this "in-between" classification. IRAS 13349+2438 (Gallo 2006) also has FWHM(Hβ) $\approx$ 2800 km s^{-1}, though its other properties are similar to NLS1s. WPVS 007 (Grupe et al. 2008a, 2008b) sometimes behaves like a NLS1, but sometimes it is undetected in X-rays. Mrk 335 (Grupe et al. 2008a, 2008b) in its low state can be considered similar to SDSS 1430−0011. All these observations suggest that the region between NLS1s and BLS1s is murky. This in-between state can be temporary in some cases, but there are also sources which usually occupy this region. Sometimes, it manifests itself as a flat X-ray spectrum (e.g., SDSS 1430−0011), sometimes as complex hard X-ray spectrum (cf. Gallo 2006), sometimes transient X-ray spectrum (e.g., WPVS 007), or simply with broad Hβ (e.g., IRAS 13349).

6. CONCLUSION

SDSS 1430−0011 appeared to show an extremely flat spectrum in the *Chandra* observation. Our subsequent *XMM-Newton* observations show that its intrinsic spectrum is steeper, with power-law slope in the normal observed range. The spectrum, however, is complex, with either a partially covering absorber or an ionized absorber, which must have varied between the *Chandra* and *XMM-Newton* observations. Based on its optical and X-ray properties, it is hard to classify SDSS 1430−0011 as either a NLS1 or a BLS1; it is at the border line between the two. There are several AGNs in this "in-between" class; SDSS 1430−0011 is not unique.

This work is supported in part by the NASA grant NNX07AQ63G to S.M. D.G. is supported in part on NASA grant NNX07AH67G.

REFERENCES

Atlee, D., & Mathur, S. 2009, ApJ, 703, 1597
Bian, W.-H., Cui, Q.-L., & Chao, L.-H. 2006, ChJAA, 6, 281
Boller, Th., Brandt, W. N., & Fink, H. 1996, A&A, 305, 53
Boroson, T. A., & Green, R. F. 1992, ApJS, 80, 109
Dickey, J. M., & Lockman, F. J. 1990, ARA&A, 28, 215
Done, C., Mulchaey, J. S., Mushotzky, R. F., & Arnaud, K. A. 1992, ApJ, 395, 275
Gallo, L. 2006, MNRAS, 368, 479
Goodrich, R. W. 1989, ApJ, 324, 224
Grupe, D. 2004, AJ, 127, 1799
Grupe, D., Leighly, K. M., & Komossa, St. 2008a, AJ, 136, 2343
Grupe, D., & Mathur, S. 2004, ApJ, 606, L41
Grupe, D., et al. 2004, AJ, 127, 156
Grupe, D., et al. 2008b, ApJ, 681, 982
Komossa, S., & Xu, D. 2007, ApJ, 667, L33
Kuraszkiewicz, J., Wilkes, B. J., Czerny, B., & Mathur, S. 2000, ApJ, 542, 692
Leighly, K. M. 1999a, ApJS, 125, 297
Leighly, K. M. 1999b, ApJS, 125, 317
Lodders, K. 2003, ApJ, 591, 1220
Makishima, K., Maejima, Y., Mitsuda, K., Bradt, H. V., Remillard, R. A., Tuohy, I. R., Hoshi, R., & Nakagawa, M. 1986, ApJ, 308, 635
Mathur, S. 2000, MNRAS, 314, 17
Mathur, S., & Grupe, D. 2005a, A&A, 432, 463
Mathur, S., & Grupe, D. 2005b, ApJ, 633, 688
Mathur, S., Kuraszkiewicz, J., & Czerny, B. 2001, New Astron., 6, 321
Mitsuda, K., et al. 1984, PASJ, 36, 741
Morrison, R., & McCammon, D. 1983, ApJ, 270, 119
Murphy, K., & Yaqoob, T. 2009, MNRAS, 397, 1549
Nikolajuk, M., Czerny, B., & Gurynowicz, P. 2009, MNRAS, in press (arXiv:0901.1442)
Osterbrock, D. E., & Pogge, R. W. 1985, ApJ, 297, 166
Page, K. L., Schartel, N., Turner, M. J. L., & O'Brien, P. T. 2004, MNRAS, 352, 523
Pfeiffer, M., Appenzeller, I., & Wagner, S. 2000, New Astron. Rev., 44, 547
Pounds, K. A., Done, C., & Osborne, J. P. 1995, MNRAS, 277, L5
Puchnarewicz, E. M., et al. 1992, MNRAS, 256, 589
Watson, L., Mathur, S., & Grupe, D. 2007, AJ, 133, 2435
Williams, R. J., Mathur, S., & Pogge, R. W. 2004, ApJ, 610, 737 (W04)
Williams, R. J., Pogge, R. W., & Mathur, S. 2002, AJ, 124, 3042 (W02)